An electrochemical biosensor with integrated microheater to improve the sensitivity of electrochemical nucleic acid biosensors

Iremnur Akcakoca[1] *(ORCID: https://orcid.org/0000-0001-9752-4190)*, Hamed Ghorbanpoor[2,3] *(ORCID: https://orcid.org/ 0000-0002-2665-8172)*, Ewen Blair[4] *(ORCID: https://orcid.org/0000-0002-1887-8001)*, Yasin Ozturk[1] *(ORCID: https://orcid.org/0000-0002-9049-0992)*, Araz Norouz Dizaji[2] *(ORCID: https://orcid.org/0000-0001-6720-2115)*, Tanil Kocagoz[5,6] *(ORCID: https://orcid.org/0000-0001-7211-2026)*, Huseyin Avci[7] *(ORCID: https://orcid.org/0000-0002-2475-1963)*, Damion Corrigan[4] *(ORCID: https://orcid.org/0000-0002-4647-7483)*, Fatma Dogan Guzel[2*] (*ORCID: https://orcid.org/0000-0001-7200-4615)*

[1]Department of Metallurgical and Materials Engineering, Faculty of Engineering and Natural Science Yildirim Beyazit University, Ankara, Turkey
[2]Department of Biomedical Engineering, Faculty of Engineering and Natural Science, Ankara Yildirim Beyazit University, Ankara, Turkey
[3]Department of Biomedical Engineering, Eskisehir Osmangazi University, Eskisehir, Turkey
[4]Department of Biomedical Engineering, University of Strathclyde, G1 1XQ, United Kingdom
[5]Department of Medical Biotechnology, Institute of Health Sciences, Istanbul, Turkey
[6]Department of Medical Microbiology, School of Medicine, Acibadem Mehmet Ali Aydinlar University, Istanbul, Turkey
[7]Department of Metallurgical and Materials Engineering & Cellular Therapy and Stem Cell Research Center, Eskisehir Osmangazi University, Eskisehir, Turkey

*Corresponding author, E-mail: fdogan@ybu.edu.tr

Abstract

Electrochemical impedance spectroscopy (EIS) is often used for biomolecular detection based on the interaction of a molecule with a receptor functionalised electrode surface and consequent impedance change. Though its performance is well established, there is still a need for improved sensitivity and specificity, especially when attempting to detect nucleic acids from clinical samples with minimal amplification steps. Localised heating is a potential approach for improving nucleic hybridisation rates and reducing non-specific interactions, and thereby producing high sensitivity and selectivity. The aim of the study was therefore to develop a microheater surrounding Au thin film electrodes, an integrated hybrid chip, for detecting genes of *Mycobacterium tuberculosis* with enhanced sensitivity. The performance of the integrated hybrid chip was determined using the changes in the charge transfer resistance (R_{ct}) upon DNA hybridisation using probe sequences for *Mycobacterium tuberculosis*. Heat transfer within the system was simulated by using COMSOL Multiphysics as a mathematical modelling tool. When a temperature of 50 °C was applied to the microheater during DNA hybridisation steps, R_{ct} values (which were indicative of DNA-DNA hybridisation) increased 236% and 90% as opposed to off-chip non-heated experiments and off-chip heated experiments. It is concluded from these observations that the microheater indeed can significantly improve the performance of the nucleic acid hybridisation assay and paves the way for the development of highly- sensitive and specific integrated label-free biosensors.

Keywords: electrochemical impedance spectroscopy, lab-on-a-chip, microheater, DNA hybridisation sensitivity

1. Introduction

Recently, development of new reliable diagnostic methodologies has received a lot of attention. In this regard, biosensors are one of the ideal candidates for use at the point of care because of their capability to monitor and evaluate chemical and biological effects by producing signals either optical, electrical, or electrochemical [1-5]. Since biosensors offer many advantages as alternatives to conventional methods, they have been employed in many scientific and industrial areas such as chemistry [6] engineering [7], biology [8] by utilising various types of bioreceptors like enzymes [9], cells [10], and aptamers [11]. Particularly, electrochemical impedance spectroscopy (EIS) can investigate in detail the relation between chemical and electrochemical effects via the passage of electric current between the solution and the electrode [12-14]. When electron transfer begins, as a result of an electrochemical reaction, the resistance of this process is called charge transfer resistance (R_{ct}) and is commonly used in biosensor measurements to determine whether the bioreceptors on the surface have successfully bound to their target [12].

Electrochemical impedance-based DNA biosensors for nucleic acid hybridisation are highly sensitive measurement tools, because, they are label-free possessing significant advantages such as not requiring extra assay steps or resources to label the target, making them lower cost, faster, and more portable over many labelled detection systems [15]. EIS-based DNA biosensors typically employ the three electrodes system which includes working, counter and reference electrodes. Electrons transfer takes place at the working electrode which is often functionalised with nucleic acid sequences or proteins [16]. There are several examples to EIS-based DNA biosensors in the literature. For example, Rainbow *et al*., reported a coft-effective and fast-responsive integrated electrochemical biosensors to detect waterbone disease [17]. Low cost and low resource micro/nano sensors was developed on flexible substrates by Bamshad *et al* [18]. Photonic crystal slab (PCS) was developed to investigate complex gases at ng level detection by Biswas *et al* [19]. Analysis of single-cell was performed with the help of the microfluidic system integrated electrical impedance by Kim *et al* [20]. Single-wall carbon nanotubes (SWCNTs) integrated glassy carbon electrode (GCE) was develop for monitoring Doxorubicin Anticancer Drug, and the limit of detection achieved 0.6 nM [21]. Detection of epithelial-mesenchymal transition (EMT) was performed electrochemical biosensors with operating quantum dot (QD) [22]. An electrochemical biosensor that operate without the need for pre-treatment was also developed for the discovery of viruses with a limit of detection of 6 μg/mL [23]. Peng *et al*., studied label-free DNA biosensors based on cyclic voltammetry and impedance spectroscopy for rapid detection of multidrug resistance MDR1 gene [24]. Blair *et al*., showed *Mycobacterium tuberculosis* detection on gold microelectrode produced through photolithography [25]. Yao et al. presented a biosensor that determined mercury ions through use of labelled nucleic acid multi-walled carbon nanotubes (MWCNTs) [26]. These studies generally employ nanoparticles, exotic electrode modification and labelled PCR systems and are therefore not amenable

to mass manufacture and therefore widespread use. In addition, selectivity and specificity issues are rarely addressed and so many promising assays do not reach maturity because of an inability to properly discriminate between specific and non-specific nucleic acid interactions, particularly in complex clinical samples.

DNA hybridisation specificity can be increased through imposition of elevated temperature, especially around the melting temperature (T_M) of the DNA duplex. Hybridisation standard free energy is low at high-temperature and therefore mismatches can be minimized [27-29]. It should be noted that these studies were carried out primarily using hybridisation simulations [30]. Zhang *et al*., investigated temperature dependent hybridisation performance by evaluating thermodynamics [27]. Javed *et al.*, manufactured a microheater platform to detect DNA attachment using a fluorescence labelled method [31]. Consequently, based on the knowledge in the field, one can conclude that elevated temperatures increase DNA hybridisation specificity. Heating effect in sensor experiments has been previously reported by several groups. Husueh *et al*., worked with microheater integrated MEMS gas sensors with blue light-emitting diode (LED) and microheater was employed to increase the temperature of sensing layer, resulting in an increase in the response of the sensor [32]. Das et al., investigated co-planar MEMS gas sensor integrated microheater to enhance the sensor response using Pt-made microheater [33]. Chen et al., developed MEMS gas sensor to detect low concentration gases and Pt-microheater was integrated to increase detection sensitivity [34]. The specific detection of gases was accomplished by microheater integrated gas sensor. In this study, by integrating a microheater alongside an electrochemical sensor, a hybrid integrated chip was produced to increase the sensitivity of DNA hybridisation. Effect of heating in electrochemical sensor experiments has also been reported in the literature. Temperature and kinetic conditions of hybridization was examined to detect single base mismatches by square wave voltammetry by Biala *et al* [35]. Electrochemical sensors with heated gold-disk electrode was performed to examine the electrocatalytic activity of horseradish peroxidase (HRP) [36]. These are rather off-chip bulk experiments. Zhang et al. developed a sensitive electrochemiluminescence (ECL) aptasensor using heated indium thin oxide (ITO) working electrode surface by applying heat via semi-integrated electrical connections [37]. In another setting, the off-chip hybridization experiment was carried out with using heated gold disk electrode immersed in water at 50°C by Reske *et al.* [38]. Flechsig *et al*. worked with heated gold disk electrode for the detection of DNA hybridization using a similar bulk experimental set-up immersed in water at 50°C, where detection limit was determined to be 3.2 nM [39]. Both of these experiments were not performed using impedance spectroscopy, but other electrochemical analysis. It is clear to us that though there are several examples on heated electrode systems for electrochemical sensor applications, to the best of our knowledge, a fully integrated micro-electrochemical sensor containing microelectrodes and a microheater on a single platform has not been presented for DNA hybridisation experiments and electrochemical impedance spectroscopy-based detection.

The goal of this study was therefore to produce simple planar chip bearing gold microelectrodes surrounded by a microheater electrode, and to investigate the effect of microheater functionality on

specific DNA hybridisation. The design and incorporation of electrodes provided an opportunity to exert control over temperature for improving assay sensitivity and specify. The results presented here showed the initial modelling and fabrication of a highly-sensitive integrated label-free biosensor, followed by characterisation of the assay performance on the system with comparison to a benchmark electrode model.

2. Materials and Methods

2.1. Oligos and chemicals

Chromium (99.99%) and gold (99.99%) used for the production of the microheater integrated electrode were purchased from Nanoovak (Turkey). Oligonucleotides were purchased from Sigma Aldrich, and the sequences are shown in Table 1. Control measurements (off-chip experiments) were performed using C223AT Screen Printed Electrodes (SPEs) with 1.6 mm gold working area purchased from Metrohm (Herisau, Switzerland). $K_4[Fe(CN)_6]\cdot 3H_2O$ (potassium ferrocyanide), $K_3[Fe(CN)_6]$ (potassium ferricyanide), 3-Mercapto-1-propanol (MCP), tris(2-carboxyethyl)phosphine (TCEP), phosphate buffered saline (PBS), sulfuric acid (H_2SO_4) were purchased from Sigma Aldrich (USA). A PalmSens-P4 potenstiostat (PalmSens, Houten, Netherlands) was used to carry out EIS measurements.

Table 1. DNA sequences used for the experiment.

Function	**Sequence (5'→3')**
Probe	[ThiC6][SP18]GGGCCCATCCCACACCGC
Complementary Target	GCGGTGTGGGATGGGCCC
Non-complementary Target	GTCTTCTTGGCGACCTCTTT

2.2. COMSOL Simulation

COMSOL 5.4 (Comsol Inc, Sweeden) was used to simulate the heat performance of the microheater using heat transfer module, AC/DC module and structural mechanics module. Multiphysics thermal expansion, temperature coupling, and electromagnetic heating were performed and physical properties of the simulation is listed in Table S1. The boundary conditions were selected for thermal expansion and temperature coupling of hybrid-chip and for electromagnetic heating of Cr-Au microheater. Electromagnetic heating equation was solved, and the simulation was performed stationary. The electric current was performed on edge of the microheater contact pad to assign heat source and the simulation was developed in air atmosphere. The mesh parameters were selected 300 µm and 200 µm for maximum and minimum element size, respectively while number of elements was determined as 4. Finally, simulations were also performed with different mesh parameters (details are given in SI and parameters are listed in Table S2).

2.3. Chip fabrication

AutoCAD 2022 (Autodesk, USA) software was then used to design the integrated hydrid chip and the shadow mask was produced from aluminium by Photofab (Cambridge, UK). The design of the chip and the fabrication procedure [40] are shown in Figure 1A and Figure 1B. The integrated hybrid chip was fabricated on 25 mm by 25 mm glass slides by thermal evaporation (NANOVAK- Turkey) through a shadow mask at Bilkent University (UNAM, Turkey) (Figure 1B-I). Glass slides and shadow mask, were cleaned with acetone and then dried with nitrogen gas. Initially, 100 nm of chromium (Cr) (99.99%) was evaporated to form an adhesion layer between glass and gold (Figure 1B-II). 300 nm of gold (Au) (99.99%) was then deposited on the adhesion layer, as shown in Figure 1B-III. After the removal of the shadow mask, the final chip was obtained, as shown in Figure 1B-IV and photography image of fabricated hybrid chip shown in Figure 1C. In order to ease the handling of the chip and provide efficient connection between the electrode/microheater contact pad and the power supply/ PalmSens, a specific chip holder was designed and manufactured from plexiglass (PMMA).

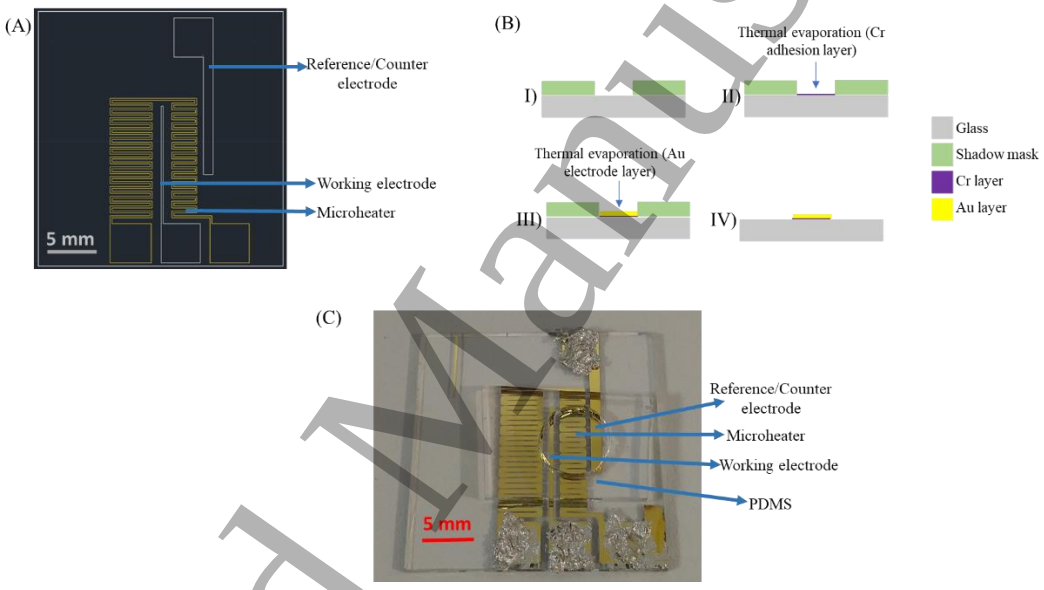

Figure 1. Schematic illustration of the design and the fabrication procedure. (A) 2D design of the hybrid chip, (B) Chip production process (I, II, III, IV), (C) photography image of manufactured chip.

2.4. Electrode functionalisation procedure

Initially, both the SPE and on-chip electrodes were cycled with 0.1 M H_2SO_4, using cyclic voltammetry (CV), to clean the working electrode surface until the cyclic voltammetry peaks were unchanging. The electrodes were rinsed with DI water for 10 s and a pre-probe measurement was performed in 1 mM ferrocyanide- ferricyanide (FF) solution in PBS. CV and EIS were performed to characterize the gold electrode surface after the cleaning. Both electrode systems were rinsed in DI water for 10 s after this measurement and a monolayer of single stranded probe DNA was attached through incubation with a probe solution containing thiolated DNA. A PDMS (polydimethylsiloxane, Slygard 184, Sigma Aldrich)-made ring was used to create a solution container on the electrode surface at the 10:1

(elastomer: curing agent) ratio. The probe solution prepared was 3 µM probe DNA with 15 µM TCEP in 1xPBS and were incubated for 16-24 h at room temperature. Then electrodes were rinsed for 10 s with DI water, dried with nitrogen respectively and were backfilled for 1 h with MCP solution. The MCP solution was prepared using 1 mM MCP, 5 mM TCEP in 1xPBS, and used to backfill the gold electrode surface which was already immobilized with probe DNA. The electrodes were then rinsed with DI water for 10 s, and post-probe measurements were performed by measuring EIS in the 1 mM FF solution. For the hybridisation step, the electrodes were rinsed with DI water for 10 s and dried with nitrogen and incubated with 100 µL of sample solution. Target incubation for complementary and non-complementary sequences was performed at 25 °C (accepted as room temperature in experiments) and 50 °C, using 500 nM target DNA 1xPBS, the electrodes were rinsed with 5 % PBS for 20 s, and the EIS measurement was performed in the 1 mM FF solution [25].

2.5. Electrochemical detection

The CV cleaning was performed between -0.5 V and 1.75 V until the oxidation and reduction peaks were unchanging. To determine the cleanliness of the electrodes, they were assessed by CV in 1 mM FF solution. Cleanliness was inferred by determining the peak-to-peak separation of the FF reduction/oxidation reaction, when measured between -0.25 V and 0.5 V. R_{ct} was extracted from the EIS measurements by fitting the data to the Randles equivalent circuit. The R_{ct} values were analysed for pre-probe, post probe and post target measurements performed in 1 mM FF solution. The EIS frequencies range was between 100 kHz and 0.1 Hz.

2.5.1 Statistical Analysis

Statistical analysis on all results was performed using paired sample t-test in SPSS software. Statistical significance threshold was set at 0.05 ($p < 0.05$). Error bars represent a standard deviation of the mean (n= 3).

2.6. Heating experiments

Heating performance of the hybrid chip was tested by changing the applied power using a power generator (22 cm x 22 cm x 7 cm) and measuring the temperature with a thermal camera (Fluke, USA). Off-chip control experiments using SPEs were performed using an incubator to provide elevated temperature (JSR, Korea).

2.7. Electrode Characterizations

AFM characterization (Quesant Q-Scope 250, Euromex Microscopen-Nederlands) was performed with a non-contact method at 49.00 µm X 49 µm scan size and 1 Hz scan rate. SEM (HITACHI SU5000, Germany) was performed gold electrode to characterize coating performance. Dektak profiler (Dektak XT Stylus Profilometer, Germany) in UNAM of Bilkent University was performed for the thickness and width characterization.

3. Results and Discussions

3.1. Heating performance of the chip

The electrodes consisted of a working and a single joint counter/reference electrode with 200 µm and 1000 µm width, respectively [41]. The microheater surrounded the working electrodes at a distance of 4000 µm while the counter/reference electrodes were placed outside the heating zone of the heater (see Figure 1A). The Dektak profiling of the electrodes showed that the overall thickness of Cr and Au electrodes was about 230 µm while the width was 1000 µm. The function of the heater was to generate and maintain the desired temperature during target hybridisation. Here, the temperature profile should be homogeneously distributed with maximum efficiency while consuming minimum energy [42]. The microheater integrated electrode – the integrated hybrid chip - was fabricated on a glass slide after the deposition of the metal electrodes. Power generator was connected to the microheater contact pads with the help of crocodile tips. Simply, the working mechanism is that the electrons collide with the atoms of the heater material (Au, Cr) with the applied current, and the heating process of the microheater takes place by transferring some of their energy to the atoms.

COMSOL Multiphysics modelling was performed three-dimensional in order to simulate the temperature distribution on the chip at 50 °C and provide an initial insight into the power/duration requirements for experimentation. This operating temperature (50 ºC) was determined as being close enough to the melting temperature of the target DNA to maximise specific and minimise non-specific DNA-DNA hybridisation [27- 30]. Simulation results obtained at 50 °C are shown in Figure 2A. The heating reached a desired maximum value of 50 °C at the centre of the working electrode. The temperature in the hybrid chip was uniformly distributed. The temperature in the circle, where the working electrode forms its centre and involves the microheater, was simulated as 50 °C (in air) and this temperature value was obtained within approximately 1 min. Heat transfer of the liquid sample and the glass substrate was disregarded for simplicity. The main goal of this study was to place the working electrode in the middle of the microheater and to benefit from the temperature distribution homogeneously. It has also been shown by COMSOL that the temperature decreases with distance from the working electrode. Furthermore, different mesh parameters were also tested. When the mesh parameters were increased from coarse to extremely fine, as shown in Table S2, there was no significant change observed. Therefore, 300 µm for maximum element size and 200 µm for maximum element size were used in all simulation studies.

Experimental results are shown in Figure 2B and Figure 2C, displaying the temperature change with applied power at 1 min and required duration to reach the desired temperature for 3 W. Power was varied from 0.29 W to 0.32 W and the duration ranged between 1 and 1.5 min. Experimentally, as seen from the figures, the power required to reach 50 °C was determined as 0.3 W (5 V – a DC current of 1.42 A). Figure 2A demonstrates the required duration for the heating to reach 50 °C and it appeared that the optimal duration was approximately 1 min. When a power of 1.68 W was applied, the chip fractured at a temperature of 158 °C, herewith the maximum temperature that the microheater can withstand has been tested.

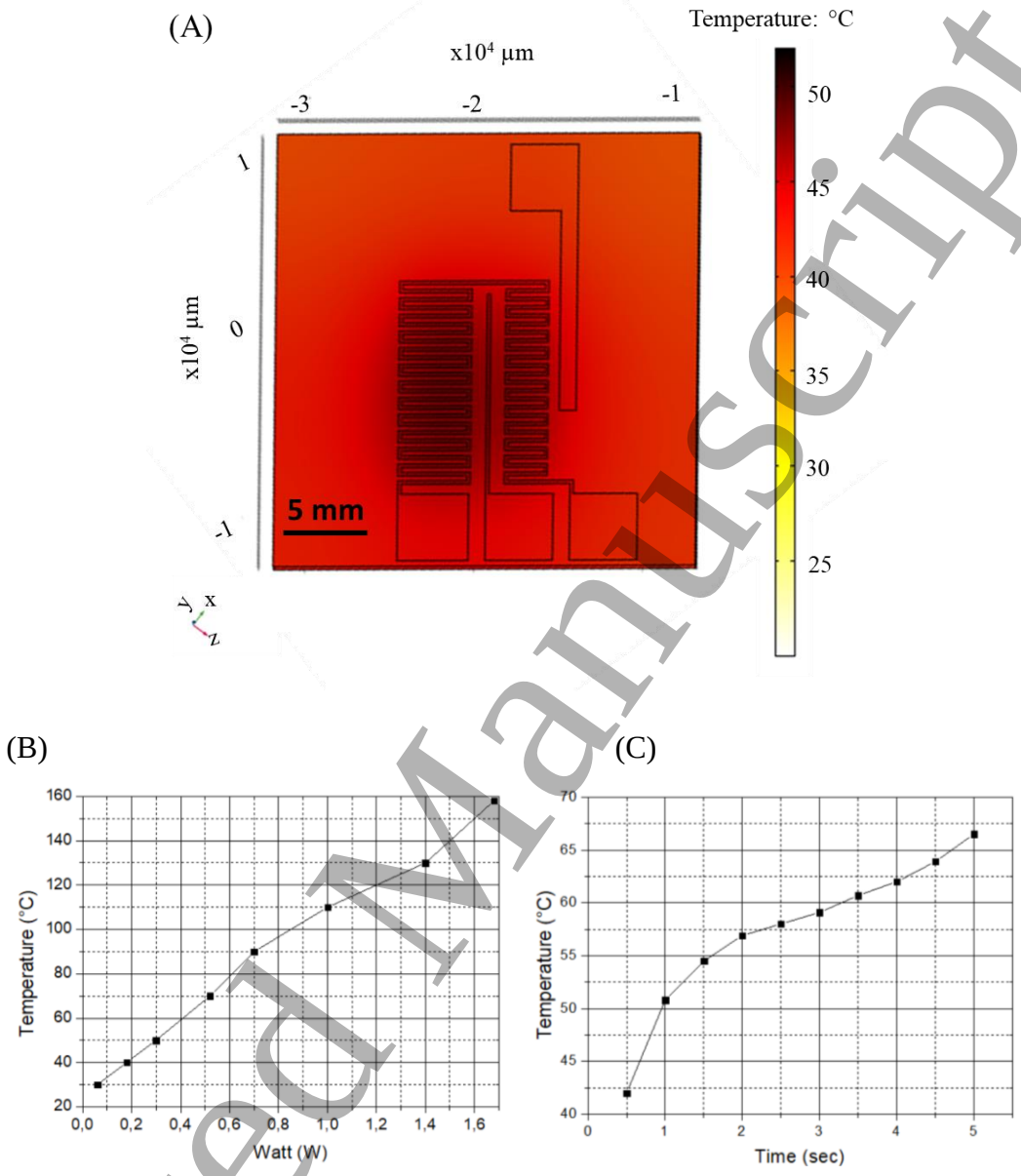

Figure 2 Simulation and experimental results. (A) Simulation graph showing the heat distribution at 50°C, (B) Experimental results showing the temperature changes with controlled power increase, (C) Experimental results showing the temperature change over time.

3.2. Electrochemical performance of chip under ambient and elevated temperatures

In the last decade, studies on biosensors have considerably increased in number and focused on improving the performance and capabilities of biosensor devices [43-45]. In the literature, nucleic acid based biosensors have been frequently reported for use under ambient conditions [46, 47]. In this study, we focused on the improvement of EIS-based nucleic acid biosensors by employing a microheater

integrated electrode chip. Experiments were divided into off-chip and on-chip. The off- chip measurements were performed using C223AT SPEs heated on an incubator and on-chip measurements were carried out using the fabricated heat generating electrodes as described above. In order to ease the fabrication procedure, both the sensing electrodes and the heat generating electrodes, the microheater were fabricated from Au and a thin Cr adhesion layer. On-chip and off-chip experiments were carried out at temperatures of 25 °C and 50 °C. The temperature of 50 °C was chosen to improve sensitivity and to decrease non-specific target hybridisation, because this temperature was close to the melting temperature of the target DNA sequence [27].

CV measurements were performed using C223AT in 1 mM FF to determine the cleaning efficacy. In off-chip experiments, the value of peak-to-peak separation was 80 mV, which is close to the ideal value of 58 mV according to the Nernst Equation, indicating that the cleaning process has been successful [48]. R_{ct} values were calculated for overall experimental steps in FF solution. The EIS outcomes are illustrated using a Nyquist plot, as shown in Figure 3A. The increasing R_{ct} value at each stage indicated that immobilization and hybridisation were successful. The EIS Nyquist plots show that the change in R_{ct} value after target hybridisation at 50 °C was higher than that observed for room temperature incubation. This suggests that hybridisation at 50 °C indeed enhanced the hybridisation sensitivity [42].

As for on-chip experiments, peak-to-peak separation was calculated to be 100 mV, which is satisfactory though larger than the SPE and the theoretical value stated above. This could in part be explained by the use of thin gold film which has slightly higher resistance than a thickly deposited gold screen printing ink. The Nyquist plots for each measurement steps are illustrated in Figure 3B and the R_{ct} values displayed show similar increases for SPEs.

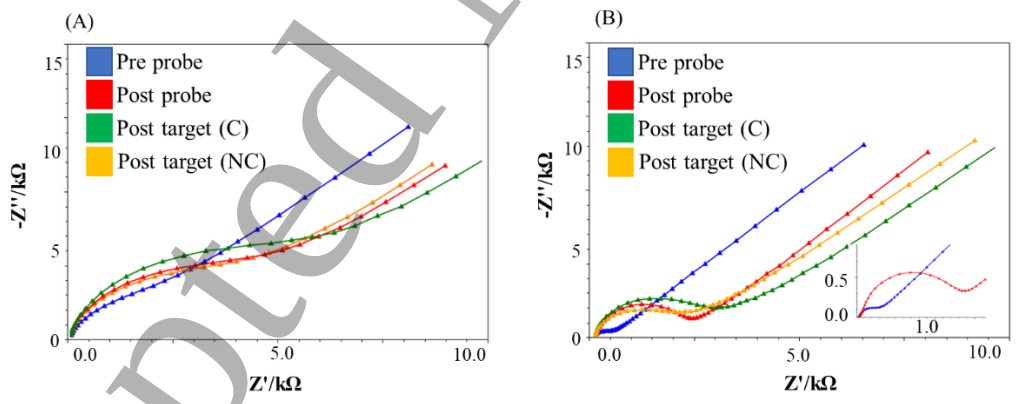

Figure 3 Nyquist plots. (A) Nyquist plot of off-chip experiments for each measurement steps, (B) Nyquist plot of on-chip experiments for each measurement steps. C; complimentary, NC; non-complimentary.

Figure 4 demonstrates signal change magnitudes for R_{ct} after complementary and non-complementary target hybridisation at different temperatures. At room temperature, the mean signal change of the SPE showed an increase of 93% while the chip response increased by 147%. This could be due to the uneven

connection of the DNA probe to the electrode surface due to the rough structure of the SPEsleading to sub-optimal hybridisation [46] or the improved electroanalytical performance offered by reducing the electrode dimensions in the hybrid chip. In short, the signal change for SPEs were less than that of the hybrid device. Our results indicate similar characteristics with the literature [50].

Hybridisation of the complementary target at 50 °C resulted in an increase of the electrochemical hybridisation signal by 236% for the chip and 146% for the SPE. This shows a higher singal change in comparison with both electrode systems at 25 °C. The increase is in line with the expectations that the incubation of target DNA close to the melting temperature of the DNA sequences of interest allows for specific hybridisation and increases the rate of hybridisation events within the sample [28-30]. These results also prove the enhanced specificity and selectivity with the use of microheater integrated electrodes, the hybrid chip and therefore higher efficacy with the microheater. There are a few studies in the literature which use microheaters. For example, Javed *et al.*, fabricated a platinum microheater platform to detect DNA using fluorescence labelling [31]. Safavieh *et al.*, reported a biosensor for real time and label-free bacteria isolation from whole blood and antibiotic susceptibility testing [51]. To achieve 37 °C for the on-chip bacteria incubation, a screen-printed heater was electrically characterized. In our study, an Au-made microheater surrounding the electrode heated at 50 °C was successfully implemented to increase the hybridisation sensitivity of nucleic acids.

Non-complementary experiments were also carried out and indicated that the probe and target binding are specific for both temperatures investigated, because changes in charge transfer resistance for the non-complementary targets are much lower than the complementary targets (Figure 4). In the case of the on-chip system, the non-complementary measurement gave a lower signal change at 50 ℃ than that at 25 ℃, indicating improved specificity of the higher temperature incubation. Therefore, the EIS results with non-complementary target confirm sensor specificity of the experiments and enhanced discrimanatory power for the assay at elevated temperature. The signal change magnitude of chip samples were more than that of SPE samples at both temperatures, which is due to the smooth and more defect-free surface of the electrodes. For most measurements, this also gave rise to a lower signal variation for the on-chip electrodes. A two-tailed t-test was performed to compare complementary and non-complementary target hybridisation signals and the outcome of the t-tests proved that there were statistically significant differences between the two, shown in Figure 4. This difference was even more enhanced when the incubation was performed at 50 ℃. Higher signal changes were also observed at 50 ℃ on the SPEs, giving confidence that incubating at higher temperature improved sensitivity.

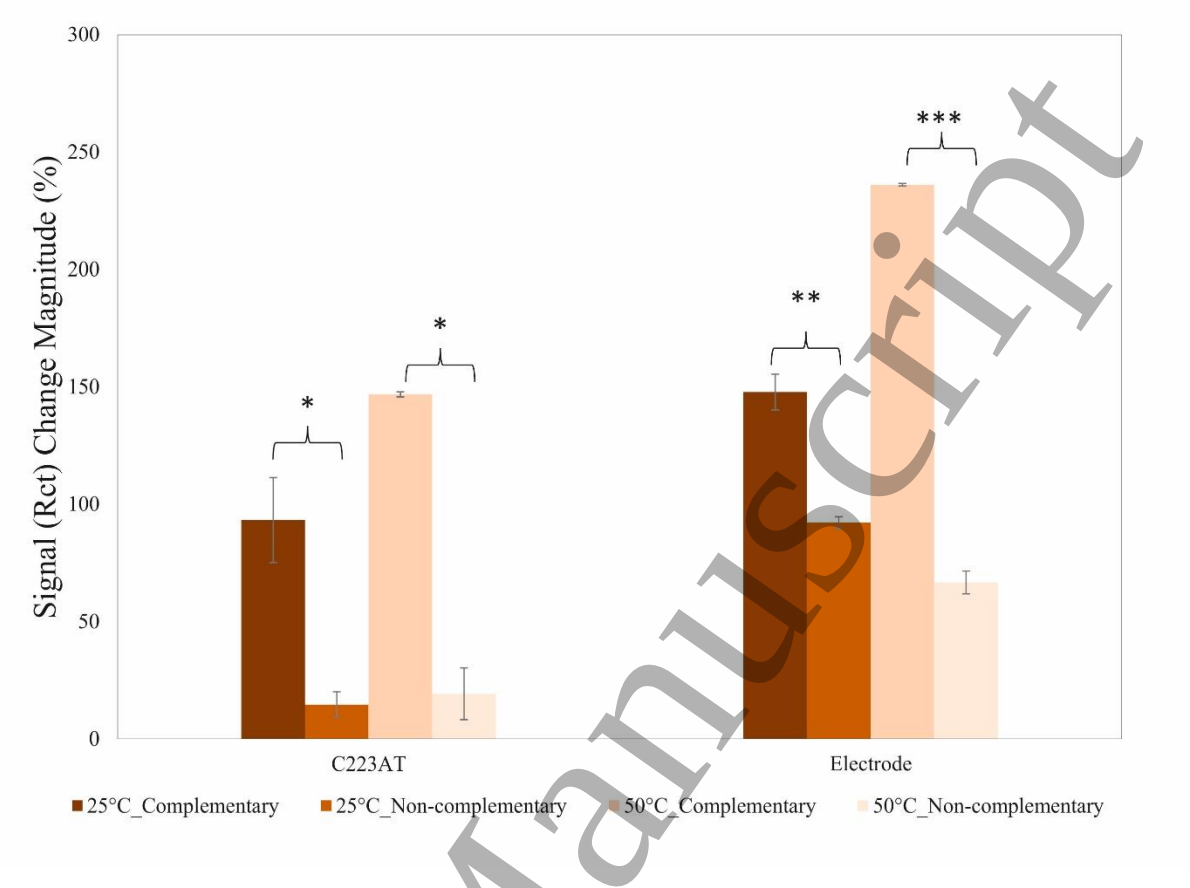

Figure 4 Signal change of SPEs (left) and hybrid chip (right) for the complementary and non-complementary targets at 25 °C and 50 °C. Error bars represent standard error of the mean (n = 3) and *p≤0.004; **p≤0,003; ***p≤0,0001 represent p-value of t-test.

3.3. Surface characterization of SPEs and the chip

Atomic Force Microscopy (AFM) was performed to evaluate surface roughness of the SPEs and the chip, as shown in Figure 5A and Figure 5B. The measurements were taken after the electrochemical cleaning of the electrode surfaces by using CV, as described above. The figures indicate that the chip has a very smooth surface in comparison with the SPEs. Root Mean Square (RMS) values were 172.5 and 7.3 nm for the SPEs and the chip, respectively, calculated from an area of 49 x49 μm^2. This indicates the surface roughness was considerably higher for the SPEs. The difference is a consequence of the rough surface of the SPE, leading to less controllable formation of the self-assembled monolayer (SAM) with more variable surface coverage than that of the smooth chip which results in the improved performance of the chip in the hybridisation experiments with non-complementary target at 50 °C [49-52].

Scanning electron microscopy (SEM) was performed to characterize surface properties of SPEs and chip (Au coating electrode). While surface roughness was observed on the SPEs surface, there was a

homogeneous distribution of Au particle on chip surface. Figure 5C and 5D were promoted sensitivity differences between SPEs and chip.

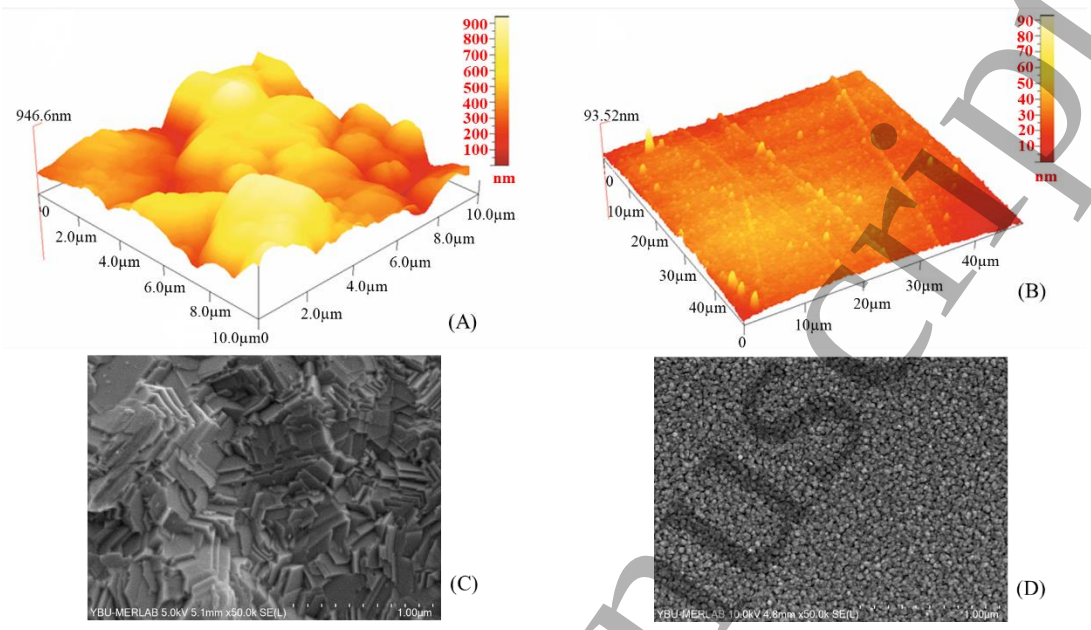

Figure 5 Atomic force microscopy images of (A) SPEs (C223AT), (B) chip and SEM figures of (C) SPEs (C223AT) and (D) chip (Au coated electrode).

4. Conclusion

In this study, we present the development of a novel microheater integrated electrode with enhanced DNA hybridisation sensitivity based on EIS experiments. The microheater electrode and the EIS electrode were both made of Au deposited on a thin Cr layer on a glass slide through a shadow mask. Production is facile and low cost because the same shadow mask can be used to produce both electrodes and there is no need for any photolithography steps. The results of the experimental heating tests were in line with the simulations, indicating that a power of 0.3 W was sufficient to reach the desired temperature, 50 °C, within a min. Sensitivity was increased about 50% and 90% when the hybrid chip was used at room temperature and 50 °C, respectively, compared to the off-chip experiments. Enhanced sensitivity and selectivity are a result of the surface properties of the electrodes, as shown by AFM images, and most importantly the use of microheater around the electrode. We believe that the concept of integrated microheater is a novel approach in improving the assay performance in not only EIS-based susceptibility assays as such, but also the on-chip biosensors in general. It will also pave the way for the development of more sophisticated and functional sensor with higher throughput.

Acknowledgement

This study was conducted in the frame of Newton Katip Çelebi Fund between Turkey and UK and supported by Turkish Scientific and Technological Council TUBITAK) under the grant number of

217S793.DC & EB acknowledge that this work was supported by a British Council Institutional Links grant, ID20180209 and delivered by the British Council. For further information, please visit www.newtonfund.ac.uk. We would like to thank Central Laboratory of Ankara Yildirim Beyazit University for allowing us to use SEM facility and Prof. Abdullah Yıldız for AFM instrumentation.

Compliance with ethical standards

Conflict of Interest No potential conflict of interest was reported by the authors.

References

References

1. D.K. Corrigan, E.O. Blair, J.G. Terry, A.J. Walton, A.R. Mount. Enhanced electroanalysis in lithium potassium eutectic (LKE) using microfabricated square microelectrodes. Anal. Chem. 86(22), 11342–11348 (2014).
2. P. Mehrotra. Biosensors and their applications–A review. J Oral Biol Craniofac Res. 6(2), 153-9 (2016).
3. E.A. Songa, J. Okonkwo. Recent approaches to improving selectivity and sensitivity of enzyme-based biosensors for organophosphorus pesticides: A review. Talanta.;155, 289-304 (2016).
4. P. Damborský, J. Švitel, J. Katrlík. Optical biosensors. Essays Biochem. 60, 91-100 (2016).
5. F. D. Güzel, H. Ghorbanpoor, A. N. Dizaji, I. Akcakoca, Y. Ozturk, T. Kocagoz, E. Blair, D.K. Corrigon, H. Avci. Label-free molecular detection of antibiotic susceptibility for Mycobacterium smegmatis using a low cost electrode format. Biotechnology and Applied Biochemistry, 68(6), 1159-1166 (2021).
6. F.D. Guzel, H. Avci. Fabrication of nanopores in an ultra-thin polyimide membrane for biomolecule sensing. IEEE Sens. J. 18, 2641-6 (2018).
7. F.D. Guzel, F. Citak. Development of an on-chip antibiotic permeability assay with single molecule detection capability. IEEE Trans Nanobioscience. 17, 155-60 (2018).
8. C. Karunakaran, R. Rajkumar, K. Bhargava. Introduction to biosensors. Biosensors and bioelectronics. Elsevier. p. 1-68 (2015).
9. D.K. Corrigan, M.J. Whitcombe, S. McCrossen, S.J. Piletsky. Pharmacology. Reichardt's dye and its reactions with the alkylating agents 4-chloro-1-butanol, ethyl methanesulfonate, 1-bromobutane and Fast Red B-a potentially useful reagent for the detection of genotoxic impurities in pharmaceuticals. J. Pharm. Pharmacol. 61, 533-7 (2009).
10. G. Baranauskas, R. Gusmeroli, A. Spinelli, C. Giordano, M.T. Raimondi. Cell-based biosensors: Current trends of the development. J Appl. Biomater. Biom. 4, 1glass-34 (2006).
11. S. Song, L. Wang, J. Li, C. Fan, J. Zhao. Aptamer-based biosensors. Trends Analyt Chem. 27, 108-17 (2008).
12. N. Elgrishi, K.J. Rountree, B.D. McCarthy, E.S. Rountree, T.T. Eisenhart, J.L. Dempsey. A practical beginner's guide to cyclic voltammetry. J. Chem. Educ. 95, 197-206 (2018).
13. A. N. Dizaji, Z. Ali, H. Ghorbanpoor, Y. Ozturk, I. Akcakoca, H. Avci, & F.D. Guzel. Electrochemical-based ''antibiotsensor''for the whole-cell detection of the vancomycin-susceptible bacteria. Talanta, 234, 122695 (2021).
14. S. O. Akbulut, H. Ghorbanpoor, B.Ö. İpteç, A. Butterworth, G. Avcıoğlu, L.D. Kozacı et al. Impedance testing of porous Si3N4 scaffolds for skeletal implant applications. Appl. Sci. 2 (2020).
15. J-Y. Park, S-M. Park. DNA hybridization sensors based on electrochemical impedance spectroscopy as a detection tool. Sensors. 9, 9513-32 (2009).

16. M.J. Afzal, M.W. Ashraf, S. Tayyaba, M.K. Hossain, N. Afzulpurkar. Sinusoidal Microchannel with Descending Curves for Varicose Veins Implantation. Micromachines. 9, 59 (2018).
17. J. Rainbow, E. Sedlackova, S. Jiang, G. Maxted, D. Moschou, L. Richtera, and P. Estrela. Integrated electrochemical biosensors for detection of waterborne pathogens in low-resource settings. Biosensors. vol. 10, no. 4, pp. 36 (2020).
18. A. Bamshad, and H. J. Cho. Laserjet Printed Micro/Nano Sensors and Microfluidic Systems: A Simple and Facile Digital Platform for Inexpensive, Flexible, and Low-Volume Devices. Adv. Mater. Technol. pp. 2100401 (2021).
19. P. Biswas, C. Zhang, Y. Chen, Z. Liu, S. Vaziri, W. Zhou, and Y. Sun. A Portable Micro-Gas Chromatography with Integrated Photonic Crystal Slab Sensors on Chip. Biosensors. vol. 11, no. 9, pp. 326 (2021).
20. S. Kim, H. Song, H. Ahn, T. Kim, J. Jung, S. K. Cho, D.-M. Shin, J.-r. Choi, Y.-H. Hwang, and K. Kim. A Review of Advanced Impedance Biosensors with Microfluidic Chips for Single-Cell Analysis. Biosensors. vol. 11, no. 11, pp. 412 (2021).
21. F. Hassani Moghadam, M. A. Taher, and H. Karimi-Maleh. Doxorubicin anticancer drug monitoring by ds-DNA-based electrochemical biosensor in clinical samples. Micromachines. vol. 12, no. 7, pp. 808 (2021).
22. X. Du, Z. Zhang, X. Zheng, H. Zhang, D. Dong, Z. Zhang, M. Liu, and J. Zhou. An electrochemical biosensor for the detection of epithelial-mesenchymal transition. Nat. Commun. vol. 11, no. 1, pp. 1-9 (2020).
23. R. M. Mayall, C. A. Smith, A. S. Hyla, D. S. Lee, C. M. Crudden, and V. Birss. Ultrasensitive and Label-Free Detection of the Measles Virus Using an N-Heterocyclic Carbene-Based Electrochemical Biosensor. ACS Sensors. vol. 5, no. 9, pp. 2747-2752 (2020).
24. H-P. Peng, Y. Hu, P. Liu, Y-N. Deng, P. Wang, W. Chen et al. Label-free electrochemical DNA biosensor for rapid detection of multidrug resistance gene based on Au nanoparticles/toluidine blue–graphene oxide nanocomposites. Sens. Actuators B Chem. 207, 269-76 (2015).
25. E.O. Blair, S. Hannah, V. Vezza, H. Avcı, T. Kocagoz, P.A. Hoskisson et al. Biologically modified microelectrode sensors provide enhanced sensitivity for detection of nucleic acid sequences from Mycobacterium tuberculosis. Sens. Actuators. 100008 (2020).
26. L. Yao, J. Teng, M. Zhu, L. Zheng, Y. Zhong, G. Liu et al. MWCNTs based high sensitive lateral flow strip biosensor for rapid determination of aqueous mercury ions. Biosens. Bioelectron. 85, 331-6 (2016).
27. D.Y. Zhang, S.X. Chen, P. Yin. Optimizing the specificity of nucleic acid hybridization. Nat. Chem. 4, 208-14 (2012).
28. R.K. Saiki, D.H. Gelfand, S. Stoffel, S.J. Scharf, R. Higuchi, G.T. Horn et al. Primer-directed enzymatic amplification of DNA with a thermostable DNA polymerase. Science. 239, 487-91 (1988).
29. L.A.G. Putra, C.J. Yonathan, N.I. Niedhatrata, M.H.R. Firdaus, J.R. Yoewono. A review of the development of Polymerase Chain Reaction technique and its uses in Scientific field. J. ilm. berk. sains terap. kim. 2, 14-30 (2020).
30. C.B. Markegard, C.P. Gallivan, D.D. Cheng, H.D. Nguyen. Effects of concentration and temperature on DNA hybridization by two closely related sequences via large-scale coarse-grained simulations. J. Phys. Chem. B. 120, 7795-806 (2016).
31. A. Javed, S.M. Iqbal, A. Jain. Microheater platform for selective detachment of DNA. Appl. Phys. Lett. 101, 093707 (2012).
32. T.-J. Hsueh, C.-H. Peng, W.-S. Chen. A transparent ZnO nanowire MEMS gas sensor prepared by an ITO micro-heater. Sens. Actuators B Chem. vol. 304, pp. 127319 (2020).
33. I. Das, R. Bhattacharyya, H. Saha, and S. Ghosh. Enhanced response of co-planar MEMS microheater-based methane gas sensor. IEEE Sens. J. vol. 20, no. 23, pp. 14132-14140 (2020).
34. M. Chen, S. Peng, N. Wang, L. Xu, F. Lin, and F. Wu. A wide-range and high-resolution detection circuit for MEMS gas sensor. IEEE Sens. J. vol. 19, no. 8, pp. 3130-3137 (2018).

35. K. Biała, A. Sedova, M. Mix, K. Böar, P. Orsag, M. Fojta, G-U. Flechsig. Amplified detection of single base mismatches with the competing-strand assay reveals complex kinetic and thermodynamic behavior of strand displacement at the electrode surface. Electrochimica Acta 285, pp. 272-283 (2018).
36. S-H. Wu, X-B. Huang, Y. Tang, L-M. Ma, Y. Liu, J-J. Sun. Temperature controllable electrochemical sensors based on horseradish peroxidase as electrocatalyst at heated Au disk electrode and its preliminary application for H2O2 detection. Analytica Chimica Acta. vol 1096, p. 44-52 (2020).
37. H. Zhang, F. Luo, P. Wang, L. Guo, B. Qiu, Z. Lin. Signal-on electrochemiluminescence aptasensor for bisphenol A based on hybridization chain reaction and electrically heated electrode. Biosensors and Bioelectronics vol 129, pp 36–41 (2019).
38. T. Reske, M. Mix, H. Bahl, and G. Flechsig. Electrochemical detection of osmium tetroxide-labeled PCR-products by means of protective strands. Talanta. vol. 74, pp. 393–397 (2007).
39. G. Flechsig and T. Reske. Electrochemical detection of DNA hybridization by means of osmium tetroxide complexes and protective oligonucleotides. Anal Chem. 79, 2125-30 (2007).
40. A. N. Dizaji, Y. Ozturk, H. Ghorbanpoor, A. Cetak, I. Akcakoca, T. Kocagoz, E. Blair, D.K. Corrigon, H. Avcı & F. D. Güzel. Investigation of the effect of channel structure and flow rate on on-chip bacterial lysis. IEEE Transactions on NanoBioscience, 20(1), 86-91 (2020).
41. A.J. Bard, L.R. Faulkner. Electrochemical Methods: Fundamentals and applications. 2nd ed. Wiley (2001).
42. R.G. Spruit, J.T. van Omme, M.K. Ghatkesar, H.H.P Garza. A Review on Development and Optimization of Microheaters for High-Temperature In SituStudies. J Microelectromech Syst. 26, 1165-82 (2017).
43. F.D. Güzel, B. Miles. Development of in-flow label-free single molecule sensors using planar solid-state nanopore integrated microfluidic devices. Micro Nano Lett. 13, 1352-7 (2018).
44. D.K. Corrigan, H. Schulze, R.A. McDermott, I. Schmüser, G. Henihan, J.B. Henry et al. Improving electrochemical biosensor performance by understanding the influence of target DNA length on assay sensitivity. J. Electroanal. Chem. 732, 25-9 (2014).
45. B. Meshginqalam, J. Barvestani. Performance enhancement of SPR biosensor based on phosphorene and transition metal dichalcogenides for sensing DNA hybridization. IEEE Sens. J. 18, 7537-43 (2018).
46. Y. Du, S. Dong. Nucleic acid biosensors: recent advances and perspectives. Anal. Chem. 89, 189-215 (2017).
47. V. C. Ruiz-Valdepeñas Montiel, E. Povedano, E. Vargas, R.M. Torrente-Rodríguez, M. Pedrero, A.J. Reviejo et al. Comparison of different strategies for the development of highly sensitive electrochemical nucleic acid biosensors using neither nanomaterials nor nucleic acid amplification. ACS Sens. 3, 211-21 (2018).
48. A. Butterworth, E. Blues, P. Williamson, M. Cardona, L. Gray, D.K. Corrigan. SAM composition and electrode roughness affect performance of a DNA biosensor for antibiotic resistance. Biosensors. 9, 22 (2019).
49. X. Wang, W. Lai, T. Man, X. Qu, L. Li, A.R. Chandrasekaran et al. Bio-surface engineering with DNA scaffolds for theranostic applications. In: Michael Hirtz, editor. Nanofabrication. De Gruyter 4, 1-16 (2018).
50. Z. Li, Y. Yu, Z. Li, T. Wu, J. Yin. The art of signal transforming: electrodes and their smart applications in electrochemical sensing. Anal. Methods. 7, 9732-43 (2015).
51. M. Safavieh, H.J. Pandya, M. Venkataraman, P. Thirumalaraju, M.K. Kanakasabapathy, A. Singh et al. Rapid real-time antimicrobial susceptibility testing with electrical sensing on plastic microchips with printed electrodes. ACS Appl. Mater. Interfaces. 9, 12832-40 (2017).
52. F. D. Guzel, I. Akcakoca, H. Ghorbanpoor, A. N. Dizaji, Y. Öztürk, E. Blair, D. Corrigan, T. Kocagöz, H. Avcı. Highly sensitive label-free electrochemical detection of heat shock protein with low-cost screen-printed electrodes. Eskişehir Technical University Journal of Science and Technology A-Applied Sciences and Engineering, 22(4), 344-352 (2021).